Atomic Physics and Radiation Processes in Plasmas
— Issues of Divertor and Disruption —

(Received – July 23, 1993)

NIFS-MEMO-11 Aug. 1993

RESEARCH REPORT
NIFS-MEMO Series

Preface

It is pointed out that atomic and molecular (A/M) processes play important roles in divertor plasmas but the problems related to these processes are not yet studied quantitatively. Recently new subjects related to A/M processes such as plasma - vapor interaction during plasma disruption are presented.

In order to profit the opportunity that Professor D. Salzmann (Soreq Nuclear Research Center, Israel) visited NIFS with Dr. H. Takabe (ILE, Osaka Univ.), a small meeting on "Atomic physics and radiation processes in divertor and/or disruption plasmas" was held on May 21, 1993 as a part of a Working Group for Atomic Processes in Plasma which is one of the activities at the Data and Planning Center in National Institute for Fusion Science. Prof. K. Itoh (NIFS) gave a review talk for the present status on A/M physics in Magnetic Fusion Research. Prof. D. Salzmann presented similarity in physical phenomena in laser produced plasmas and disruption plasmas. Dr. H. Takabe explained a structure of hydro-radiation codes used for laser produced plasmas.

This is a brief summary of our discussions. Our recent results of the calculations for the line emissions of carbon atoms in edge plasmas are also included.

Takako KATO
Data and Planning Center
National Institute for Fusion Science

Keywords;
atomic processes, radiation, divertor plasmas, disruption plasmas,
high density plasmas

Contents

Some Problems Related to A/M Physics in Magnetic Fusion Research

K. Itoh
National Institute for Fusion Science

In this note, some processes, which is important but is not conventionally analysed, is discussed in relation with the A/M physics in toroidal plasmas.

1 Major Disruption

The major disruption is one of the key issues in the magnetic confinement fusion research. The physics of the disruption phenomena has been studied from various point of view. At present, the four phases of the disruption are distinguished, and each phase requires the relevant physics modelling.

(1) The first phase is that the plasma is subject to the slow change of current profile, so that the profile turns to those which are unstable against low-n MHD modes (n: toroidal mode number). [Time scale of the order of 10ms-1sec.]
(2) The second phase is characterized by the growth of the low-n mode. [1-10ms.]
(3) In the third phase, the electron temperature crashes in the whole plasma column. [10-100μs.]
(4) In the fourth phase, the plasma current decays and the one turn loop voltage shows a positive spike, generating very energetic electrons.

The A/M physics is particularly important in understanding the phases (1) and (4). The transport of the impurities are considered to shrink the current profile, through radiation cooling of the edge, and to destabilize the low-n mode.

The more drastic role seems to be played by A/M physics in the final phase of the disruption.

This phase, among the four, has the largest impact in the engineering aspect of the tokamaks. The large loop voltage V_ℓ causes the runaway electrons. These electrons can have the energy of 10-100MeV in large tokamaks, and cannot be stopped at the surface of the first wall of the vacuum chamber. Secondly, the mirror image current is enhanced by the large V_ℓ, and the image current on the wall gives rise to the tremendous mechanical force on the vacuum chamber. The reduction of the positive loop voltage spike at the disruption is an urgent task.

The loop voltage is proportional to $d[L_pI_p]/dt$ (L_p: inductance of the plasma, I_p: plasma current). The decay time of the plasma current is dictated by the resistive skin time of the plasma, $\tau_R = L_p/R_p$ (R_p: plasma resistance). The short decay time is realized by the large plasma resistance. Thus the loop voltage is proportional to R_p and we have

$$V_\ell \propto Z_{eff}T_e^{-3/2}.$$

The experimental observations yield that the decay time of the main plasma current can be as short as 1ms. The relevant electron temperature for this fast decay is below 10eV.

The mechanism of the plasma cooling thus has a key impact on the development of the disruption event. The destruction of the magnetic surface by the development of the low-n mode is one of the origins of the rapid temperature decay. However, the anomalously-enhanced thermal conductivity under the condition of the braided magnetic surface is considered to satisfy the

relation

$$\chi \propto \sqrt{T}.$$

This relation explains the rapid decay of the high temperature plasma, but is not effective to cool the cold plasmas. It is found, according to simulation, that this transport process is not enough to cool the plasma below 100 eV.

The cooling by the radiation of impurities is highly influential for the low temperature plasmas. If one writes the radiation density as $P_{rad} = n_e n_I L_I$ (n_e: electron density, n_I: impurity density), the relation

$$dL_I/dT_e < 0$$

often holds for the low temperature plasmas.

The key issue is then the determination of the rate of impurity influx into the main plasma. For this purpose, the analysis is far from satisfactory. For instance, the rate of the power deposition on the wall, which would be influenced by the evaporated impurities, has not been completely modeled. The mechanism of the impurity motion into the plasma is not clarified yet. [Is it in a from of neutrals?] The screening effect of scrape-off layer plasma has not yet been quantified.

Though the physics picture has not been established, the important role of the A/M process has been, at least indirectly, demonstrated experimentally. For instance, when the wall material is replaced from carbon to beryllium, the rate of the current decay was much prolonged under some circumstances. The coefficient L_I for the latter material is effective at very low temperature, so that the decay of T_e from $\sim$100eV to $\sim$10eV could have been decelerated in case of the beryllium wall. Other efforts has been done to change the length of the scrape-off-layer plasma. When the length of the scrape-off layer plasma becomes longer, the probability of the ionization in the scrape-

off-layer plasma is increased, and the penetration into the core plasma may be resisted. The experimental result in this trial was affirmative.

These result encourages the researches on the A/M physics related to the major disruptions.

2 Improved Confinement

The importance of the A/M physics in this area has been even less recognized. However, I believe that there is a key A/M process related to the phenomena of the enhanced plasma confinement.

The experimental mystery is that the plasma confinement time is strongly dependent on the wall conditioning process. For instance, the change of the wall material from carbon to boron was effective in increasing the energy confinement time. This was partly expected that the lighter impurities less radiate in the plasma of the keV range, so that the radiation loss from the core plasma would be reduced. The reduction of the radiation was confirmed. The surprise was that the main reason in the improvement in the energy confinement time is the reduction of the conductivity, not the suppression of the radiation loss.

The similar and mysterious observation was also made on the device with metal wall. When the devise, which was operated with the partial SUS wall, was completely carbonized, the plasma density profile was found to change. The reflection energy of the neutrals from the wall is more energetic in the case of SUS in comparison with carbonized wall. However, the penetration length of the neutrals from the wall is, in both cases, much much shorter than the plasma minor radius. The slight difference eventually causes the difference in the transport coefficient: the pinch term seems different in these discharges.

These fact will have a large impact in the fusion research. For instance, the project of the fusion experimental reactor will meet the problem. The engineering phase of such a device requires the first wall which is consist of metals. This is because the large amount of the neuron fluence. The problem of the tritium inventory will also require the solution of the metallic wall. On the contrary, the present database, in particular for the enhanced confinement mode, is restricted to the case of the low-Z wall. The compatibility of the good confinement and the nuclear test should be crucial problem in future.

Some theory has been made to explain these observations. However, the understanding is very limited. Lot of efforts should be paid in this direction of the fusion research. I would suggest that the 'physics of impure plasmas' provides a wide and uncultivated arena for the future of plasma physics.

DIVERTOR-PLASMA INTERACTIONS

David Salzmann

The ITER power and particle control systems are based on a double null poloidal divertor, made of the rather high-sputtering-threshold low$-Z$ graphite, or graphite based materials. Its main purpose is to remove about $200MW$ of alpha heating power, at an operational lifetime of the order of one year, with minimum contamination of the plasma by high-Z ions.

Present day simulations predict that the divertor will operate at a rather low temperature of $30eV$, and edge density of $\geq 4 \cdot 10^{13} cm^{-3}$. The total power incident on the plates is roughly $100MW$, additional $100MW$ is carried by the radiation, of which $60MW$ are bremsstrahlung and $40MW$ as impurity line emission. Under these conditions the outer surface of the divertor will be slightly vaporized and one may expect a gradual density and temperature changes from "room" temperature solid state density near the divertor surface, to very low density ($\sim 10^{14} cm^{-3}$) and rather high temperature ($\sim 50eV$) in the outer portions of the vapor.

During disruptions the divertor, and other plasma facing components, will experience a burst of $500MJ$ energy within quench time of a few milliseconds. In the disruption phase runaway electrons having energy as high as $300MeV$ may hit the divertor.

Both under steady state or disruption conditions the details of the vapor expansion may play important role, and the hydrodynamics of the vapor evolution has to be taken into account.

Simulations of the performance of the ITER tokamak divertor has been carried out by two-dimensional computational models which include detailed treatments of the important atomic, molecular and surface processes. Results from these computational models were compared with tokamak experimental data with limiters and divertors. The database, however, is insufficient to resolve many of the modelling uncertainties.

The physics of the plasma -divertor interactions both in the steady state and disruption operations have a few stages:

(i) First, the plasma particles, obliquely incident electrons and ions, penetrate into the outer low density parts of the vapor surrounding the divertor, see Fig.(1a). These particles lose their energy to the low density ionized vapor by a dE/dX mechanism, thereby heating the outer layers of the vapor. This heating occurs to

within a depth which equals the oblique range of the particles inside the vapor. Additional heating is carried out by the incident radiation whose mean free path and penetration length into the vapor are longer than those of the charged particles. As the main part of the incident particles energy is transformed into ionization + kinetic energy of the vapor electrons , there may be a difference between the electron and ion temperatures in this region.

Eventually, as a result of the continuous bombardment of the outer portions of the vapor by ions and electrons from the tokamak plasma , the vapor will consist of a mixture of carbon, deuterium, tritium and helium ions, each having an ionization state which is characteristic to the local plasma density and temperature .

(ii) Second, the electrons and the ions in the vapor exchange their energy by electron -ion collisions, thereby equilibrating the temperature between these two kinds of particles. As the rate of equilibration depends on the electron -ion collision rate, which on the other hand depends on the local densities , the electron and ion temperatures are expected to be equal at the higher density layers but not necessarily at the lower density ones.

(iii) At a rather narrow part inside the vapor, where the temperature is still rather high, but the ion density is not too low, the conditions are optimal for radiation emission. As in any plasma , the emission consists of the bremsstrahlung (free-free), recombination (free-bound) and line (bound-bound) radiations. The radiation propagating away from the divertor will be, on its greater part, be lost. The radiation propagating to the direction of the divertor will be absorbed partly in the vapor and partly by the divertor, thereby heating the dense vapor layers and the divertor.

(iv) The electrons from the heated vapor also transfer energy into the deeper parts in the vapor, and to the divertor surface, by electron heat conduction. This process produces a temperature gradient between the outer hot portions of the vapor and the inner dense but cooler parts which are closer to the divertor surface.

A sharp phase transition between the solid and vapor states occurs at the layer where the local temperature and pressure are suitable for the melting of a layer of atoms from the solid substrate. Deeper inside the divertor temperature gradients and heat conduction proceed into the solid substrate.

All these processes have analogy to laser plasma interactions, which are successfully simulated by computer codes in various laboratories. In fact, except for the first step, namely the energy deposition step, all the other processes are similar to those taking part in laser- plasma interactions, see Fig.(1b). Other differences between the two interaction schemes are connected to the different temperature and density scales in the two

kinds of plasmas . The interesting density and temperature domains in laser produced plasmas span the region of $10^{18} - 10^{23} cm^{-3}$ and $10 - 3000eV$, whereas the corresponding regions in plasma -divertor interactions are $10^{14} - 10^{23} cm^{-3}$ and $0.026 - 50eV$. These differences may be important in selecting the databases used for the computations, but otherwise the processes for the plasma -divertor physics can be inferred from the well investigated computer codes of laser-plasma physics.

It seems therefore plausible that a computer code used to simulate laser plasma interaction can, with the appropriate modifications, be applied also to simulate the divertor-plasma interactions.

The differences in the temperature and density domains in the two cases require, however, an investigation whether the available databases for the various atomic and radiative processes can cover the regime for plasma -divertor interactions as well. Table I lists the various models to be used in the four above mentioned regions of the divertor vapor, and the availability of databases required for these regimes. This table includes also remarks as to what extent can the existing laser- plasma codes adequately describe the underlying physics or, perhaps, need modifications.

The prevailing conditions in the low density outer *coronal region* are densities between $10^{14} - 10^{16} cm^{-3}$ and rather constant electron temperature of about $50eV$. The ion temperature is lower, and is generally unimportant. As the electron and ion densities are relatively low, the system in this part reaches a steady state at rather long times. Therefore, the atomic physics in this region, namely charge state distributions, electron density and radiation emission rates, has to be computed by means of a system of time-dependent rate equations. While routines for the solutions of these equations are used in some ultra-short laser produced plasmas, they are not in common use and need development for the divertor case. The other two main databases, for radiation transport and equation of state (EOS), are relatively simple in this region. Radiation transport can be safely neglected, as the plasma is transparent in its low density portion. An ideal gas type EOS can describe the pressure at this low density case with sufficient accuracy.

The *interaction zone* spans the region where the density changes between $\sim 10^{16} - 10^{18} cm^{-3}$, while the electron temperature is still rather constant, $\sim 10eV$. The *heat conduction zone* spans deeper portions. In this region the plasma is heated mainly by electron heat conduction and the temperature drops from the rather constant temperature in the outer part, to about $\sim 1eV$ while the density increases to $10^{18} - 10^{22} cm^{-3}$. The existing models of atomic physics, particularly the *Collisional Radiative Model (CRE)*, can adequately describe the charge state distribution and radiation rate in this domain. The databases for EOS are also well developed: one can use either the SESAME tables or the QEOS model, both provide sufficient accuracy. On the other hand, the theory of the radiation transport of the continuous spectrum while being well understood is a

rather difficult problem, and its inclusion into a simulation code may substantially increase the computational time. The inclusion of the line spectrum transport may, however, impose even more serious theoretical and computational difficulties. The heart of the difficulty is that line spectra emitted at various density and temperature conditions of the vapor may have shifted line centers and different widths than the corresponding absorption lines. Possible solution can be the inclusion of only one or two most important lines in the transport, or even the omission of any of them.

Near the *divertor-vapor interface region* temperatures are around the carbon melting point, $\sim 0.25eV$, and the solid/vapor density is about $10^{23}cm^{-3}$. This is the region where the solid evaporation and the vapor resolidification are taking place, therefore there is special importance for a careful simulation of the physical processes in this region. The radiation transport in this part is rather simple: a $T^3 \mathrm{grad}T$ type radiation diffusion routine can adequately describe the process. The EOS package is also rather simple, although the correct low temperature constitutive relations of the divertor material must be used. The high density atomic physics package, however, is not yet developed for this high density low temperature regime, and needs special preparations. Such a package can be prepared by using Thomas-Fermi or more sophisticated models. The preparation of such a database requires a few months.

Altogether, it seems that the modelling of the ITER divertor physics can be improved by using ideas borrowed from laser- plasma interactions, and a laser- plasma simulation code, with the appropriate modifications, can be applied to describe the divertor physics as well.

Table I : Databases for PLASMA - DIVERTOR INTERACTION simulations

		Atomic Physics : charge states, $\overline{Z}$, radiation	Status	Radiation Transport	Status	EOS, Pressure ($\overline{Z}$)	Status
Outer Corona	$T \sim 50$ eV $n \sim 10^{14}$—10^{16} cm^{-3}	time dependent rate eq's.	needs new routines	transparent	√	ideal gas	needs adjust-ment
Interaction Zone	$T \sim 10$ eV $n \sim 10^{16}$—10^{18} cm^{-3}	Collisional-Radiative Model	√	Continuous spectrum	√	SESAME, QEOS &c...	√
Heat Conduction Zone	$T \sim 1$ eV $n \sim 10^{18}$—10^{22} cm^{-3}	CRE (LTE)	√	Line spectrum	√		
Divertor - vapor Interface	$T \sim 0.05$ eV $n \sim 10^{23}$ cm^{-3}	High density atomic physics	to be deve-loped	Black-body transport T^3 grad T	√	Solid state EOS	needs correc-tions

(a) divertor-plasma interaciton

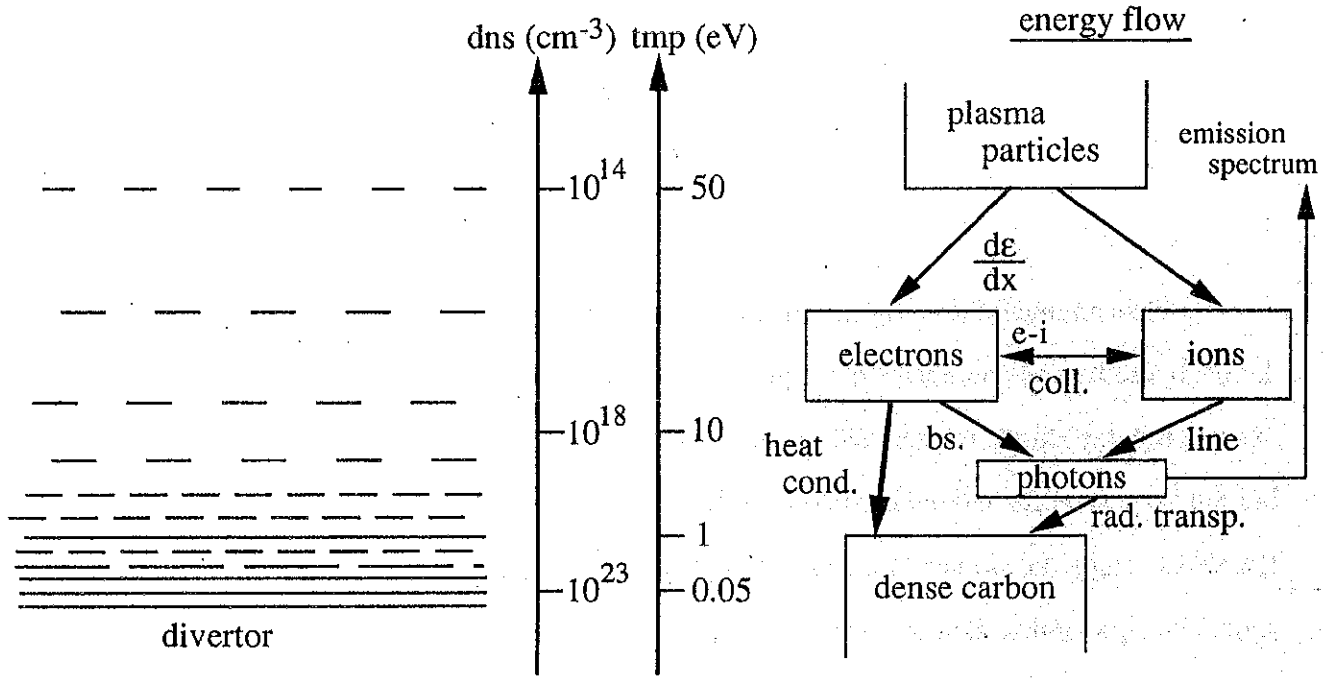

(b) laser-plasma interaction

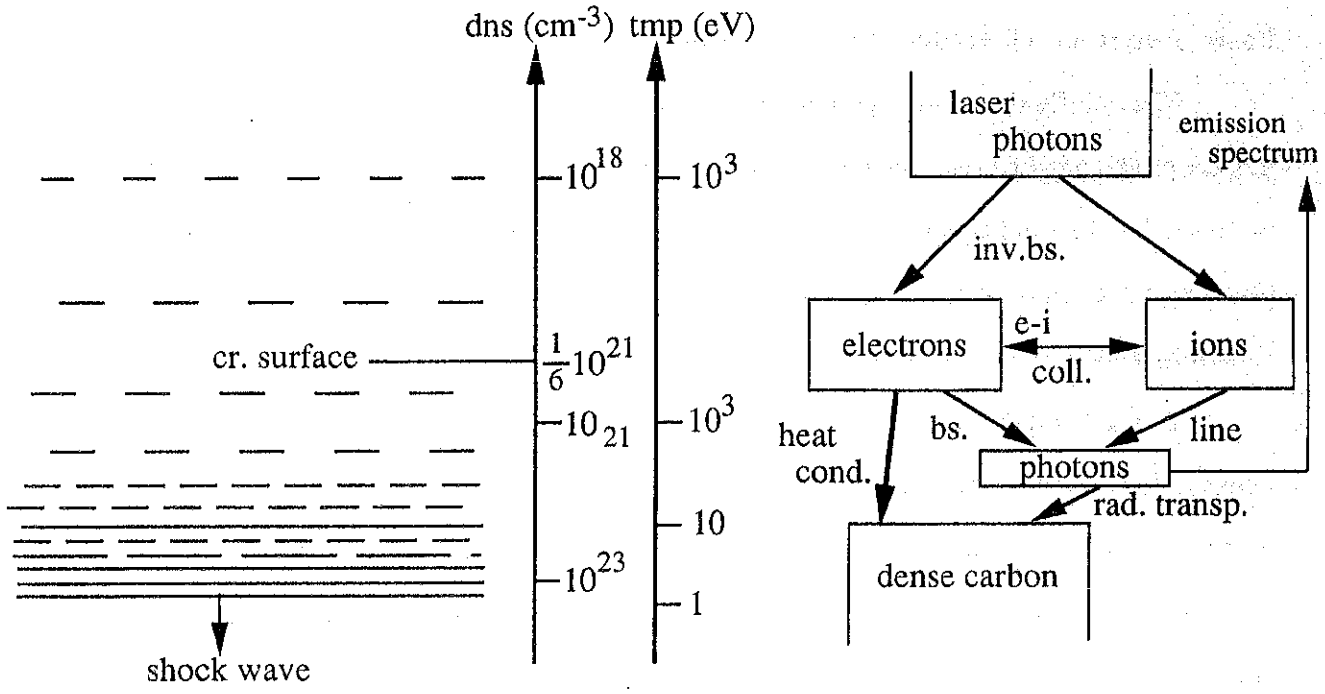

Fig. 1 : The basic elements of the (a) divertor-plasma, and (b) laser-plasma interactions

Structure of Hydro-Radiation Code

H. Takabe

Institute of Laser Engineering, Osaka University

2-6 Suita, Osaka 565

When an intense laser light is irradiated on a material, vaporization and ionization take place to drive a hydrodynamic motion of the material. When the intensity is not high enough to fully ionize the material, the atomic process and the equation of state become an important issue to be studied. For the purpose of the inertial confinement fusion (ICF) research, we have developed a code ILESTA to study the atomic state and hydrodynamic phenomena in laser produced plasmas. There should be a possibility to apply such a hydrodynamic code to study the ablation phenomena of material surface when a disruption of magnetically confined core plasma occurs. In the note, we briefly describe the basic equation solved in the code and the structure of the code. Atomic properties of carbon plasma used in the code are also shown.

Basic Equation of Hydro-Radiation Code

The one-fluids, two-temperature model is usually used to describe hydrodynamic phenomena in laser produced plasmas. The most of the coefficients used in the model are based on, for example, those used in the fluid equations of Ref.[1]. The effect of radiation heating and cooling of the plasmas is evaluated by coupling the equation of radiation transfer with the fluid equations. The basic equations solved in the hydro-radiation code ILESTA are shown in Fig.1.

In Fig.1, Eqs.(1) and (2) are the equation of continuity and motion and, ρ, $\mathbf{u}$, and p are the density, flow velocity and total pressure ($p = p_e + p_i$), respectively. In Eq.(2), Q represents the numerical viscosity, which plays substantial role at the shock wave front. Equations (3) and (4) are the equations of ion and electron energies, respectively. In solving Eqs.(3) and (4), the left hand sides are solved by replacing as

$$\frac{d\varepsilon_k}{dt} = \frac{\partial \varepsilon_k}{\partial T_k}\frac{\partial T_k}{\partial t} + \frac{\partial \varepsilon_k}{\partial \rho}\frac{d\rho}{dt} \qquad (8)$$

where k = i, e. In Eq.(3), q_i is the ion heat condition, Q_{ei} is the electron-ion temperature relaxation term proportional to $(T_e - T_i)$, and $S_\alpha{}^i$ is the alpha-particle heating term, although this term is not necessary for the present problem.

In Eq.(4), ε_e represents all the electron internal energy per unit mass of the plasma. In general, ions are not fully ionized and ε_e consists of the contributions from free electrons and bound electrons. In Eq.(4), q_e is the nonlinear electron heat conduction, S_L is the laser heating term, S_r is the sum of radiation heating and cooling contribution, and $S_\alpha{}^e$ is the alpha particle heating term. Equation (5) represents the radiation transport equation for the radiation intensity $I^\nu(t, \mathbf{r}, \Omega)$ where ν, c, and Ω are radiation frequency, the speed of light, and the vector of radiation propagation in a unit solid angle. In Eq.(5), η^ν and χ^ν are spectral emissivity and opacity, respectively. In solving Eq.(5), radiation energy $h\nu$ is divided into about 100 groups and the so-called multi-group flux limited diffusion model is used. In general, the qausi-stationary state ($\partial / \partial t = 0$) is a good approximation to Eq.(5) and S_r of Eq.(4) is given as

$$S_r = -\int\left(\eta^\nu - \chi^\nu I^\nu\right)d\Omega d\nu \qquad (9)$$

Equation (6) represents the kinetic equation to the alpha-particle, but we do not describe about this equation here. Equation (7) represents the laser propagation and absorption. In the divertor physics, Eq.(7) should be replaced by an equation to charged particles with an appropriate stopping power formula [2]. The situation is similar to the ion beam material interaction problem.

When the material is low-Z and laser (energy source) intensity is high enough, the plasma can be approximated by fully ionized ideal gas. However, for the case of the low intensity energy source or high-Z material such as gold, the plasmas are partially ionized and in non-LTE (nonlocal thermodynamic equilibrium) state. In this case, sophisticated calculation of the equation of state (EOS) and radiation transfer become important in plasma hydrodynamic motion. In addition, it becomes important to determine the ion charge state Z*. The relation described by the equations of Fig.1 is shown in the form of diagram in Fig.2.

Finally it should be noted that in the situation of low intensity such as $10^{7\text{-}10}$ W/cm^2, and a long time duration of energy source ($\sim\mu$sec), the present numerical method, explicit method, to solve Eq.(2) is not convenient because Courant-Friendrichs time step limitation is so severe. A new

method, therefore, will be required to apply the ILESTA to the material surface ablation, by low intensity, long time duration energy source.

Equation of State

In partially ionized plasma, we have to evaluate the form of p_e, p_i, ε_e, ε_i, Z^* as functions of (ρ, T_e) or (ρ, T_i). The Thomas-Fermi model [3] is famous of a statistical model to describe atomic states of high density matter. In ICF simulation, the SESAME table of Los Alamos National Lab. [4] has been frequently used as EOS table. This table is partly empirical, while mainly based on the Thomas-Fermi model.

However, it is not convenient to use the table in the hydro-code, because the physics model used in SESAME is not so clear and the ICF research requires a wide range of the values of (ρ, T). It is convenient to use a fitting formula derived from some reasonable physical model.

The EOS of the fitting formula should over all temperature and density and should tend to the EOS of the ideal gas at high temperature and low density limit and the Fermi gas EOS at high density and low temperature. In addition, it should also reproduce the properties of solid material, such as bulkmodulas and molecular bonding effect, near the solid density and room temperature.

Since in ICF a variety of material is used for targets, it is convenient if the fitting formula is applicable to any kind of materials by replacing several parameters. The QEOS [5] has been developed for such a purpose. The QEOS employs the Cowan model [6] for the ion component and the formula to the ion free energy is given by dividing the region into three ; namely, low temperature solid for $T_i < \theta_D$, high temperature solid for $\theta_D < T_i < \theta_m$ and fluid phase for $\theta_m < T_i$, where θ_D is the Debye temperature and θ_m is the melting temperature. As for the electron component, the Thomas-Fermi model is used and a modified Morse-type potential is added to include the molecular bonding effect [7].

In the ILESTA code, we use the fitting formulas given in Ref.[8], the basic idea of which is the same as QEOS. It should be noted that when the pressures and internal energies are given directly as a form of fitting formula, the thermodynamic consistency

$$\frac{p_k}{\rho} - \rho\frac{\partial \varepsilon_k}{\partial \rho} = \frac{T_k}{\rho}\left(\frac{\partial p_k}{\partial T_k}\right) \qquad (k = e, i) \qquad (10)$$

should be satisfied [9]. Then, using Eqs.(8) and (10), Eqs.(3) and (4) are solved as the equations of the ion and electron temperatures with given forms of p_k, $\partial\varepsilon_k / \partial T_k$ and $\partial p_k / \partial T_k$ as functions of (ρ, T_k), where k = e, i.

Finally, it should be noted that the QEOS and related formulas are based on the Thomas-Fermi model which is essentially the LTE (local thermodynamic equilibrium) model. In non-LTE situations, we have to use some different methods to determine the thermodynamic properties of the plasmas and this can be done by considering some atomic model to describe the partially ionized state. Brief guide line of non-LTE plasmas is given below relating to the plasma opacity and emissivity calculation.

Atomic State and X-ray Radiation Transfer

The atomic state and the EOS should be consistent each other. However, the Thomas-Fermi model does not provide the reasonable state of bound electrons and we need a further calculation to obtain the spectral opacity and emissivity.

In partially ionized plasmas, the bound-free and bound-bound radiation transfer becomes important. In order to evaluate the spectral opacities and emissivities, the detail information about change distribution of the ions including their internal electronic configuration is required. The average atom model such as the Thomas-Fermi model is not directly used to evaluate material opacities and emissivities. Therefore, evaluation of η^ν and χ^ν requires sophisticated calculations. In addition, we have to solve the equation of radiation transfer [Eq.(5) in Fig.1] to obtain the coupling term S_r with the electron fluid.

In considering the atomic state and radiation transfer, we can divide the issue into three ; atomic model, rate equation, and radiation transfer. In what follows a brief explanation on these three is described by referring to the diagram of Fig.3.

The atomic model means the way to calculate the energy levels and wave functions of bound electrons in an atom for a given electronic configuration. The simplest model is the SHM (Screened Hydrogenic Model) and is used widely in ICF research [10]. The original SHM gives energy levels of the state n (principal quantum number) averaged over splitted ℓ states. Recently improved models are proposed to include the ℓ-splitting effect [11].

If the atom is of low Z, we can also use more detail calculation such as MCDF [12]. In case of partially ionized carbon plasma, MCDF data or even experimental data can be used to obtain

energy levels and rate coefficients. Then, situation is rather simple compared to the higher-Z plasma such as gold which is of great interest in ICF.

We have to calculate the population $p_{\zeta,m}$ of the ions in charge state ζ and internal electronic state m. In obtaining $p_{\zeta,m}$, the rate equation to $p_{\zeta,m}$ should be solved. There are essentially three ways to obtain $p_{\zeta,m}$. In case of LTE, the Fermi-Dirac distribution can be used to obtain $p_{\zeta,m}$ for given energy levels $\varepsilon_{\zeta,m}$ and statistical weight $g_{\zeta,m}$. As the result, the SE (Saha equilibrium) is obtained. In low density plasmas, however, the radiative decay becomes important and the CRE (collisional radiative equilibrium) appears to be more reasonable [13]. This model covers SE at high density, low temperature region and CE (Coronal equilibrium) at low density, high temperature regions. The third way is to solve the rate equation directly. This is required when the change of temperature and density is relatively faster than the characteristic times of rate coefficients. In the divertor plasma, this should be done in the outer corona region as pointed out by Salzmann in this report.

Once the population $p_{\zeta,m}$ is obtained, the spectral opacities and emissivities can be calculated with given oscillator strengths and energy levels. In this case, however, the opacity by line radiation is not so simple because of a variety of line broadening effects at high density and low temperature. The statistical method such as UTA and STA [14] is not applicable to low-Z case such as carbon. We need to obtain each line profile with an appropriate line shape. May be we can pick up several lines which can be considered to be most important in energy transport. Then, it is enough to treat in detail the radiation transfer of only these lines. The radiation transfer should be calculated by dividing each of line profile of these lines into a few tens of groups including wing region.

Carbon Atomic State

For reference, we show charge state and charge distribution obtained by using the average atom model of R.L. More in Ref.[10], which is used in the ILESTA. In Fig.4, the equi-contours of the effective charge Z* (the average number of free electrons per ion) of carbon plasma are plotted for the LTE state and the CRE state in the range of 10^{-8} g/cm^3 < ρ < 1 g/cm^3 (cf : $\rho = 10^{-8}$ g/cm^3 corresponds to $n_i = 5\times10^{14}$ cm^{-3}) and 2 eV < T_e < 100 eV. By comparing both of them, it is seen that the CRE coincides with the LTE in high density and low temperature region, while they differ in high temperature and low density region. In the former region, the collisional processes are

predominant compared to the radiative recombination and de-excitation processes and the detail balanced LTE state appear even in the CRE model. In contrast, in the latter region the radiative recombination and de-excitation play an important role to reduce the number of free electrons as seen in the CRE result of Fig.4. It should be noted that the helium-like carbon whose effective charge $Z^* = 4$ is populated in the wide range in the (ρ, T_e) diagram.

By following the statistical method described in Ref.[15], we have calculated the charge distribution of the carbon plasma of $n_i = 5 \times 10^{16}$ cm^{-3} as a function of electron temperature. In Fig.5, the cases of the LTE and the CRE are shown. This result is consistent with the average charge state Z^* of Fig.4. Since the helium-like carbon exists in the wide range, the detail opacity calculation of the helium-like configuration will be required for the present problem.

References

[1] S.I. Braginskii, in **Review of Plasma Physics** edited by Leontovich (Consultant Bureau, New York, 1965), Vol.1, p.205.

[2] for example ; E. Nardi, E. Peleg and Z. Zinamon, Phys. Fluids **21**, 574 (1978).

[3] Ya.B. Zel'dovich and Yu. P. Raizer, **Physics of Shock Waves and High-Temperature Hydrodynamic Phenomena** (Academic, New York, 1966) Chap.III.

[4] T4-group, Los Alamos N. Lab. Rep. LALP-83-4 (1983).

[5] R.M. More et al., Phys. Fluids **31**, 3059 (1988).

[6] R.D. Cowan, Phys. Rev. **105**, 144 (1956)

[7] C. Kittel, **Introduction to Solid State Physics**, 5-th ed. (John Wiley & Sons, New York, 1976) Chap. 3.

[8] K. Takami and H. Takabe, Tech. Rep. Osaka Univ. **40**, 159 (1990).

[9] R.L. More, **Atomic Physics in ICF**, Lawrence Livermore Lab. No.UCRL-84991 (1981). Chap.IV.

[10] R.M. More, J.Q.S.R.T **27**, 345 (1982) ; J.C. Slater, Phys. Rev. **36**, 57 (1930) ; H. Mayer, **Method of Opacity Calculations**, Los Alamos Scientific Lab. Reprint LA-647, Los Alamos, 1947.

[11] F. Perrot, Physica Scripta **39**, 332 (1989).

[12] for example ; P. Grant, B.J. McKenzie, P.H. Norrington, D.F. Mayers and N.C. Pyper, Comp. Phys. Commun. **21**, 207 (1980).

[13] D. Salzmann and A. Krumbein, J. Appl. Phys. **49**, 3229 (1978).

[14] J. Bauche, C. Bauche-Arnoult and M. Klapisch, Phys. Rev. **A20**, 2424 (1979) ; A. Bar-Shalom, J. Oreg, W.H. Goldstein, D. Shvarts and A. Zigler, Phys. Rev. **A40**, 3183 (1989).

[15] H. Takabe and T. Nishikawa, **Computational Model for Non-LTE Atomic Process in Laser Produced Plasmas**, to be published.

Figure Captions

Figure 1 Basic equations solved in the hydro-radiation code ILESTA.

Figure 2 Diagram indicating the relations between fluid and radiation elements solved in the ILESTA code.

Figure 3 Diagram of calculation of atomic state and radiation transport.

Figure 4 Equi-contours of the effective charge, the average number of free electrons per ion, of carbon plasma. LTE and CRE represent the results obtained by the models of local thermodynamic equilibrium and collisional radiative equilibrium, respectively.

Figure 5 The fraction of ions in different charge states of carbon plasma for the case of $n_i = 5 \times 10^{16}$ cm^{-3} as a function of temperature. LTE and CRE represent the results of local thermodynamic equilibrium and collisional radiative equilibrium models, respectively.

$$\frac{d\rho}{dt} = -\rho \nabla \mathbf{u} \tag{1}$$

$$\rho \frac{d\mathbf{u}}{dt} = -\nabla (p + Q) \tag{2}$$

$$\rho \frac{d\varepsilon_i}{dt} = -(p_i + Q)\nabla \mathbf{u} - \nabla \mathbf{q}_i + Q_{ei} + S_\alpha^i \tag{3}$$

$$\rho \frac{d\varepsilon_e}{dt} = -p_e \nabla \mathbf{u} - \nabla \mathbf{q}_e - Q_{ei} + S_L + S_r + S_\alpha^e \tag{4}$$

$$\frac{1}{c}\frac{\partial I^\nu}{\partial t} + \Omega \nabla I^\nu = \eta^\nu - \chi^\nu I^\nu \tag{5}$$

$$\frac{\partial}{\partial t}\phi^\alpha + \mathbf{v}\nabla\phi^\alpha = \left(\frac{\partial \phi^\alpha}{\partial t}\right)_{coll} \tag{6}$$

$$\mathbf{v}_g \nabla I_L = -\nu_{abs} I_L \tag{7}$$

Fig.1

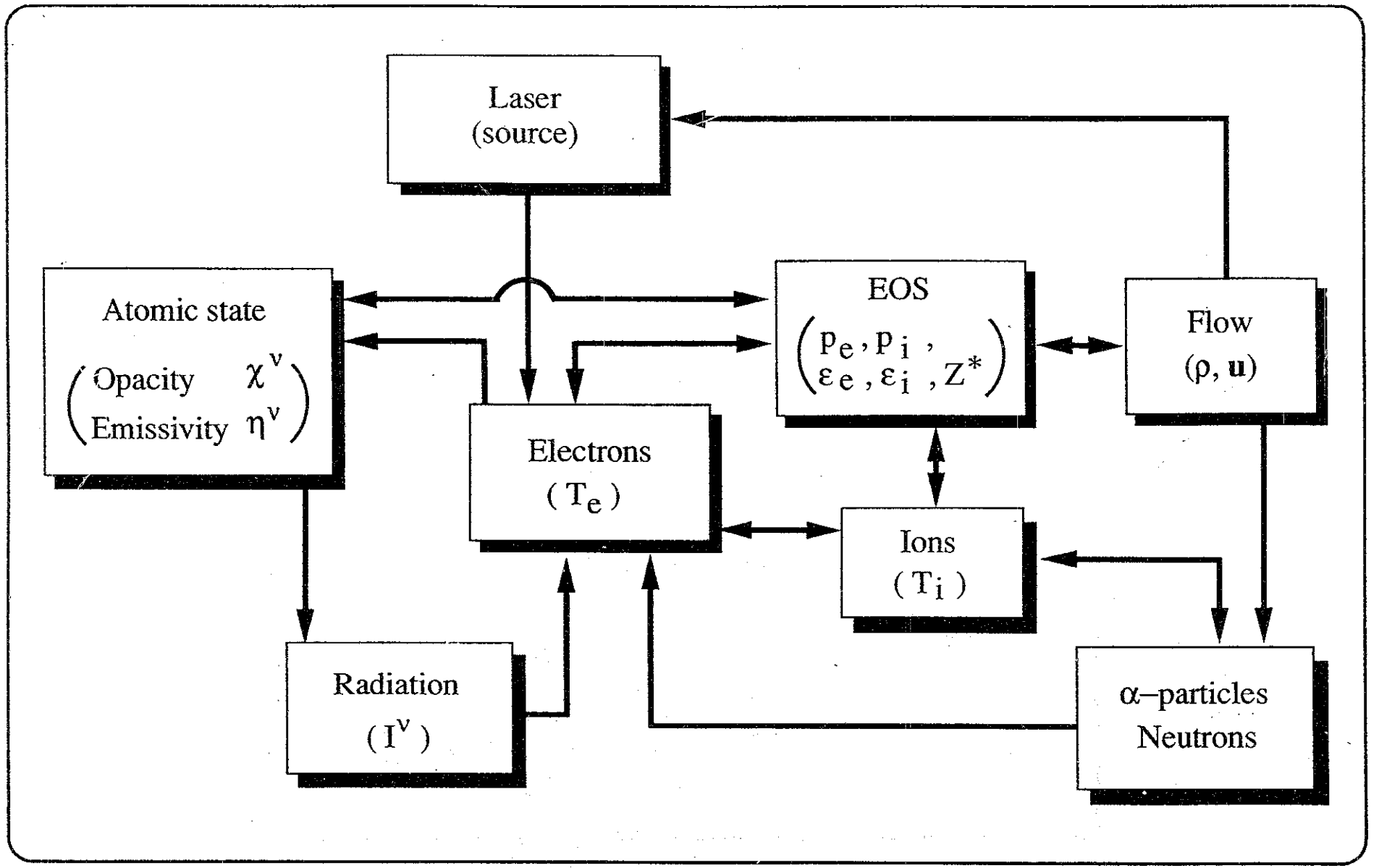
Laser
(source)
Atomic state
Opacity χ^{ν}
Emissivity η^{ν}
EOS
$p_e, p_i,$
$\varepsilon_e, \varepsilon_i, Z^*$
Flow
$(\rho, \mathbf{u})$
Electrons
(T_e)
Ions
(T_i)
Radiation
(I^{ν})
α–particles
Neutrons

Fig. 2

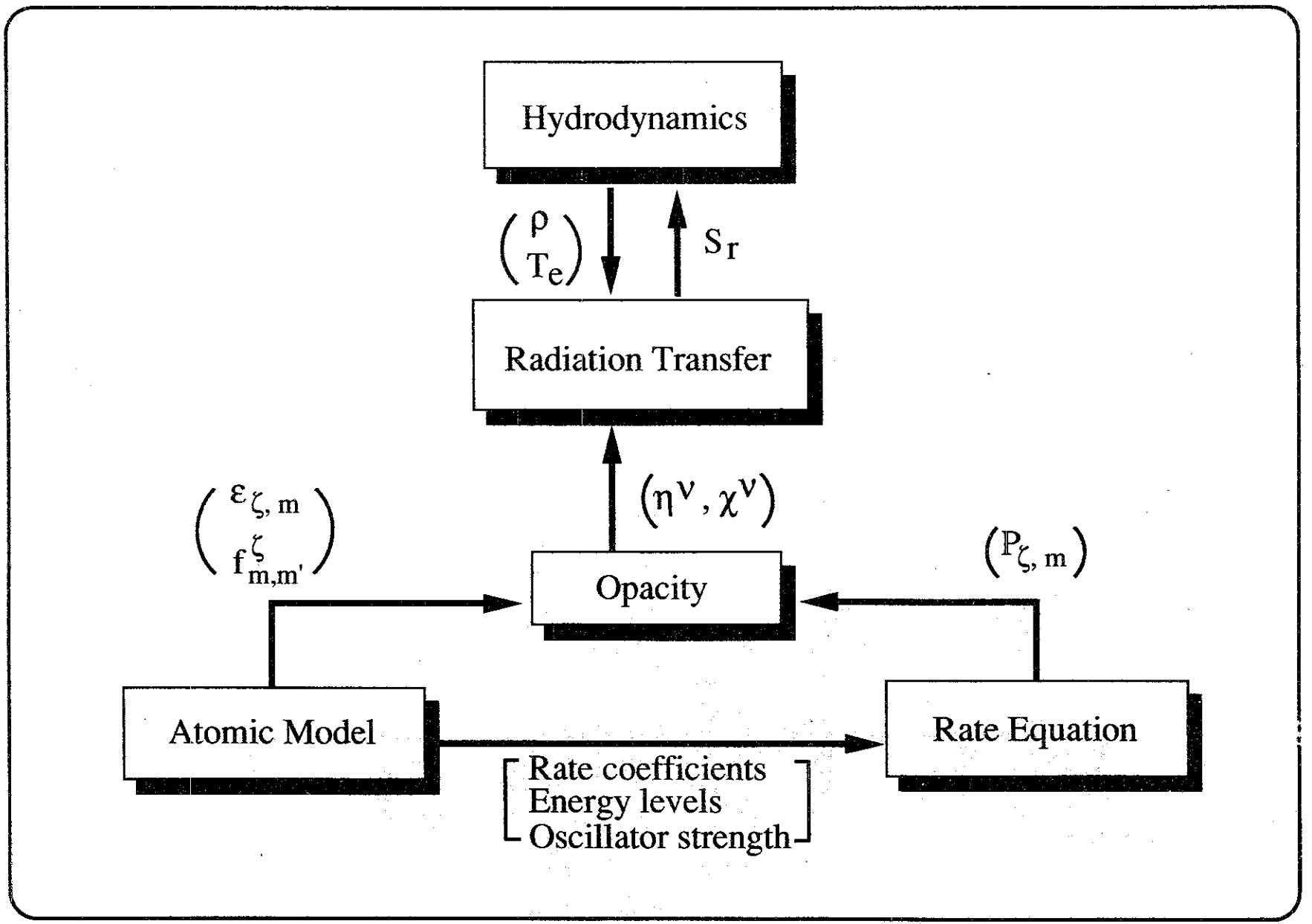
Hydrodynamics
$\begin{pmatrix} \rho \\ T_e \end{pmatrix}$
S_r
Radiation Transfer
(η^ν, χ^ν)
$\begin{pmatrix} \varepsilon_{\zeta, m} \\ f^{\zeta}_{m,m'} \end{pmatrix}$
Opacity
$(\mathbb{P}_{\zeta, m})$
Atomic Model
Rate Equation
Rate coefficients
Energy levels
Oscillator strength

Fig. 3

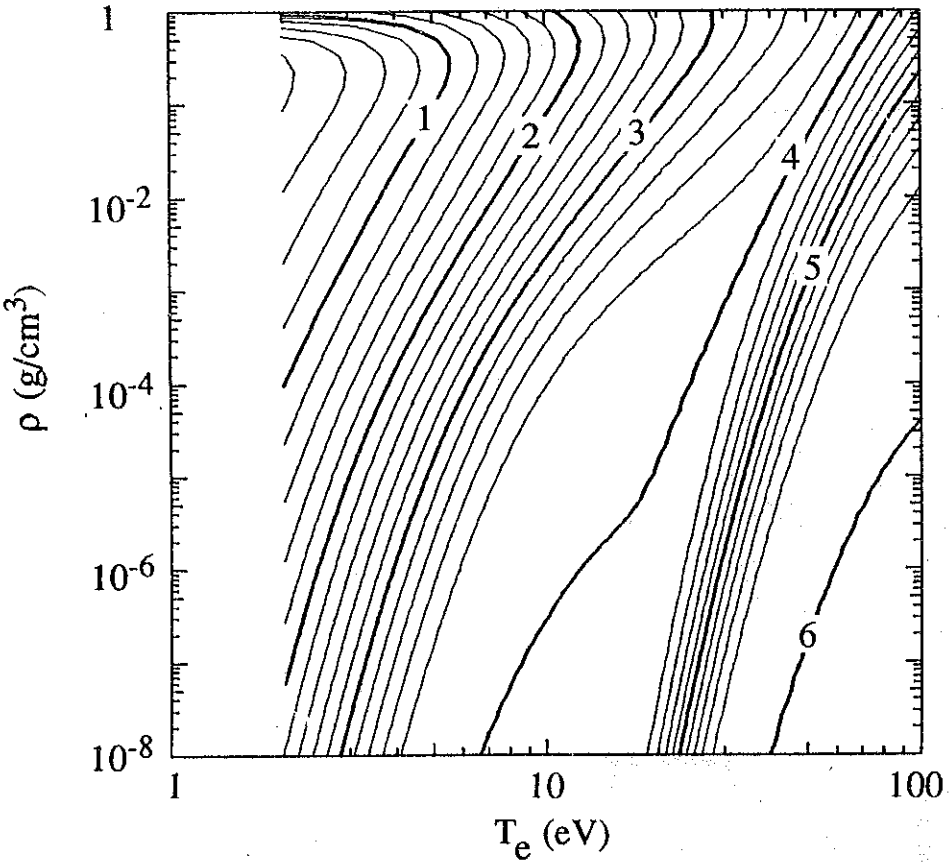
1
10^{-2}
10^{-4}
10^{-6}
10^{-8}
ρ (g/cm^3)
1
10
100
T_e (eV)
1
2
3
4
5
6

CRE

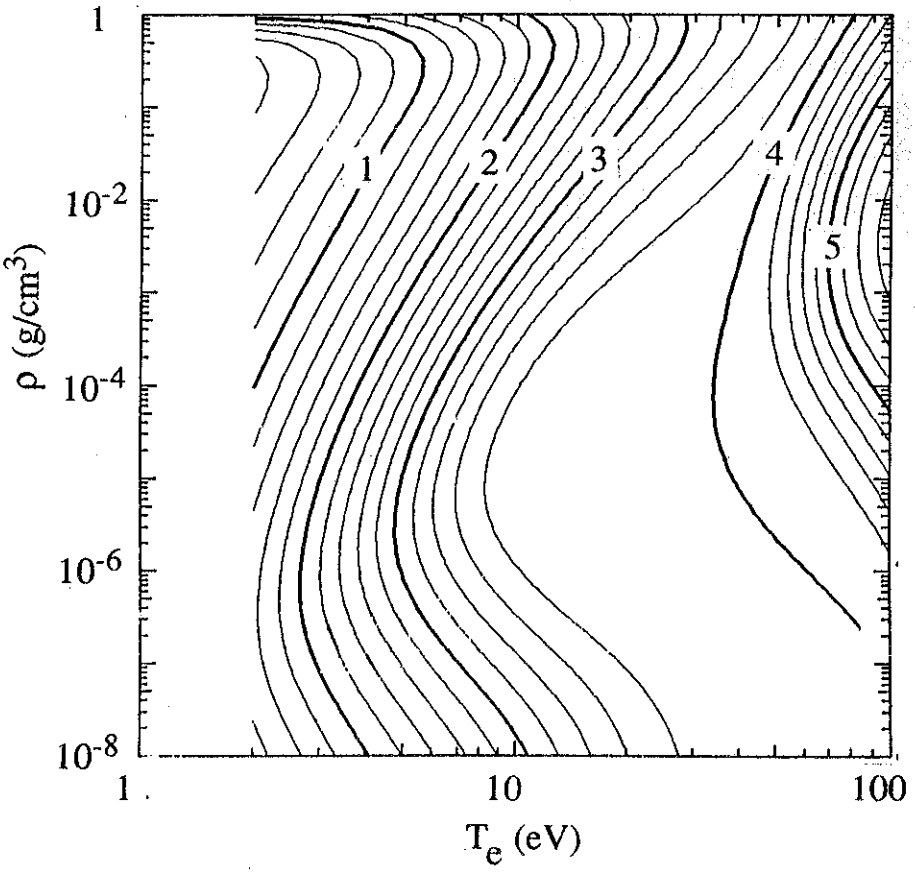
1
10^{-2}
10^{-4}
10^{-6}
10^{-8}
ρ (g/cm^3)
1
10
100
T_e (eV)
1
2
3
4
5

Fig. 4

[$\rho = 10^{-6}$ g/cm^3, $n_i = 5 \times 10^{16}$ cm^{-3}]

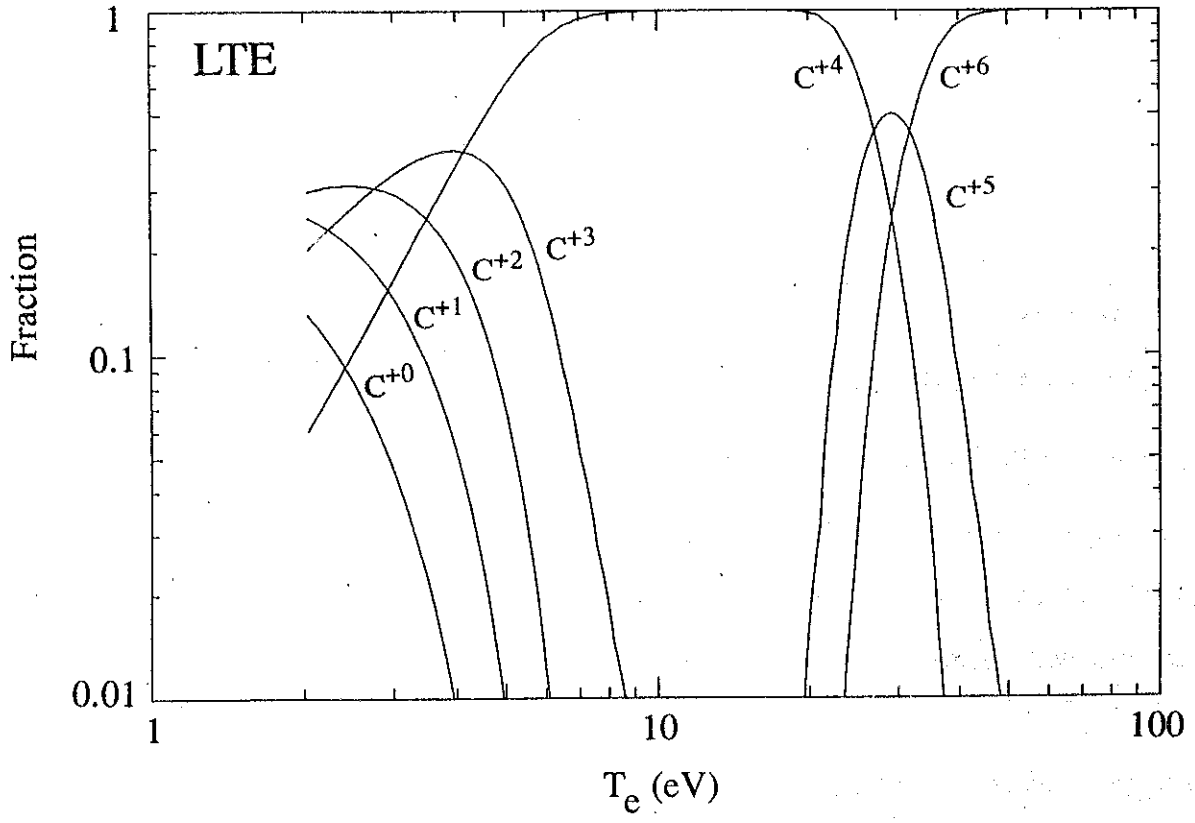

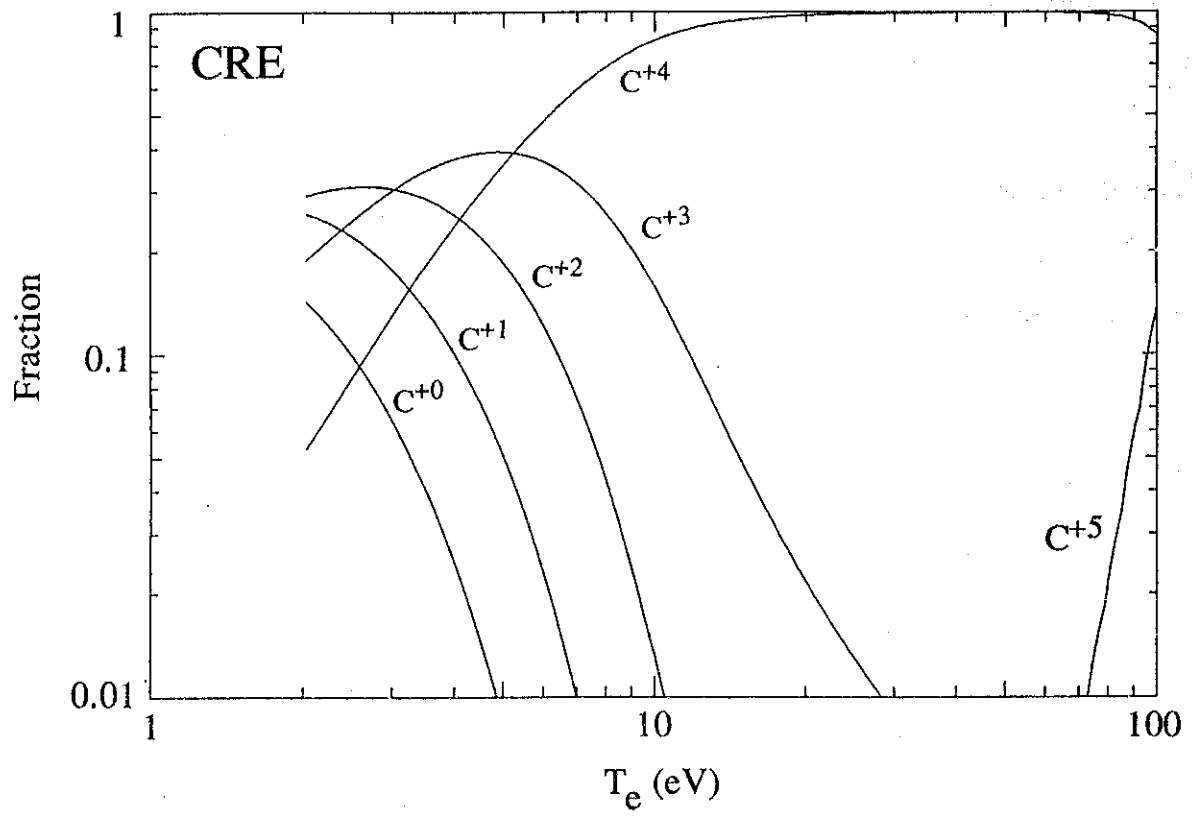

Fig. 5

Line Emissions from Carbon Atoms in an Ionizing Plasma

T. Kato

National Institute for Fusion Science

Emissions from carbon atoms have been studied mainly for the forbidden transitions from metastable states in low temperature plasmas up to now. We have investigated[1] the line emissions from carbon atoms under the condition of an ionizing plasma for the diagnostics purpose in divertor plasma where the electron temperatures are rather high comparing to the ionization potential of carbon atoms. We present here some of the results.

1. Energy levels of carbon atoms

In Fig.1 the energy level diagram is shown for the levels of n = 2, 3 and 4. The typical line transitions for UV and visible regions are shown as arrows in Fig.1.

2. The population densities

The population densities are calculated including all the transitions; the radiative transitions A_{ij}, electron excitations C_{ij}, de-excitations C_{ji} and ionizations S_i. The ionizing plasma is assumed in our model. The population densities of the excited levels n(i) depend on the electron densities and temperatures of the plasmas. Since the transition probabilities A_{ij} from the metastable states ($2p^2\ ^1S$, $2p^2\ ^1D$ -> $2p^2\ ^3P$) are very small comparing to the allowed transitions, the population densities of the metastable states begin to be determined by only the collisional processes from the electron densities n_e greater than 10^5 cm^{-3} as shown in Fig.2. The populations of the metastable states influence those in the singlet terms. The

population densities in n = 3 levels begins to be constant from $n_e = 10^{13}$ cm^{-3}.

3. Line emissions

The effective emission rate coefficients $C^{eff} = n(i)A_{ij}/(n_e \Sigma n(m))$ for the five lines which transitions are indicated in Fig.1 are shown in Fig.3 as a function of the electron temperature T_e. The lines in the singlet terms (247.9nm, 538.0nm) decrease toward higher electron temperatures. The effective emission rate coefficients of all the lines decrease for the increase of the electron density n_e, since the population densities are nearly constant for $n_e > 10^{13}$ cm^{-3}.

The radiation power rate coefficient including all the 91 line emissions are shown in Fig.4 as a function of the electron temperature. The radiation power increases as the electron density increases proportionally at low densities but saturates for $n_e > 10^{14}$ cm^{-3} .

4. Effective ionization rate coefficients

Although the effective emission rate coefficients C^{eff} generally decrease as the electron density increases, the effective ionization rate coefficient

$$S^{eff} = S_i\{n(i)\ (\Sigma_k S_{ik})\}/\Sigma_m\ n(m)$$

increases with high densities since the ionization rate coefficients from excited states are much higher than that from the ground state. As shown in Fig. 5, the n_e dependence of the effective ionization rate coefficients is relatively large at low temperatures.

5. Opacities

We estimate opacities for carbon emissions. The optical depth τ can be

written as $d\tau = kdL$, where k is the absorption coefficient, L is the pathlength. $k = \sigma(\lambda_0)N$ where $\sigma(\lambda_0)$ is the cross section of the absorption at the line center λ_0 and N is the density of the atoms. In the plasmas where the Doppler broadening is dominant as the spectral broadening,

$$\sigma(\lambda_0) = (\pi e^2/m_e c) f\lambda_0 (M/2kT\pi)^{1/2} = 1.08 \times 10^{-16} f\lambda_0 (A/T_i)^{1/2}$$

where f is the oscillator strength, A is the mass number, λ_0 is the wavelength in A and T_i is the ion temperature in eV. In the uniform density and temperature plasmas, $\tau(\lambda_0) = \sigma(\lambda_0)NL$ where NL is the column density. In Fig.6 the optical depths are plotted as a function of the column density for the resonance line of carbon atoms (1657A) for ion temperatures 1eV and 100eV. The optical depths for Lyα of hydrogen atoms (1216A) are also shown by dashed lines for comparison. For the column density of 10^{13} cm^{-2}, the opacity for carbon atoms can not be neglected.

References

1. Y. Ohkouchi, S. Sasaki, S. Takamura and T. Kato, NIFS-228(1993)

Figure Caption

Fig. 1. Energy levels of carbon atoms.

Fig. 2. Population density ratios n(i)/n(1) as a function of electron density (a) and electron temperature (b).

Fig. 3. Effective emission rate coefficients for the lines of atomic carbons.

Fig. 4. Line radiation power rate coefficient in eV cm^3 s^{-1}.

Fig. 5. Effective ionization rate coefficients for atomic carbons in an ionizing plasma.

Fig. 6. Optical depth for the lines of C I 1657A and H Lyα 1216A.

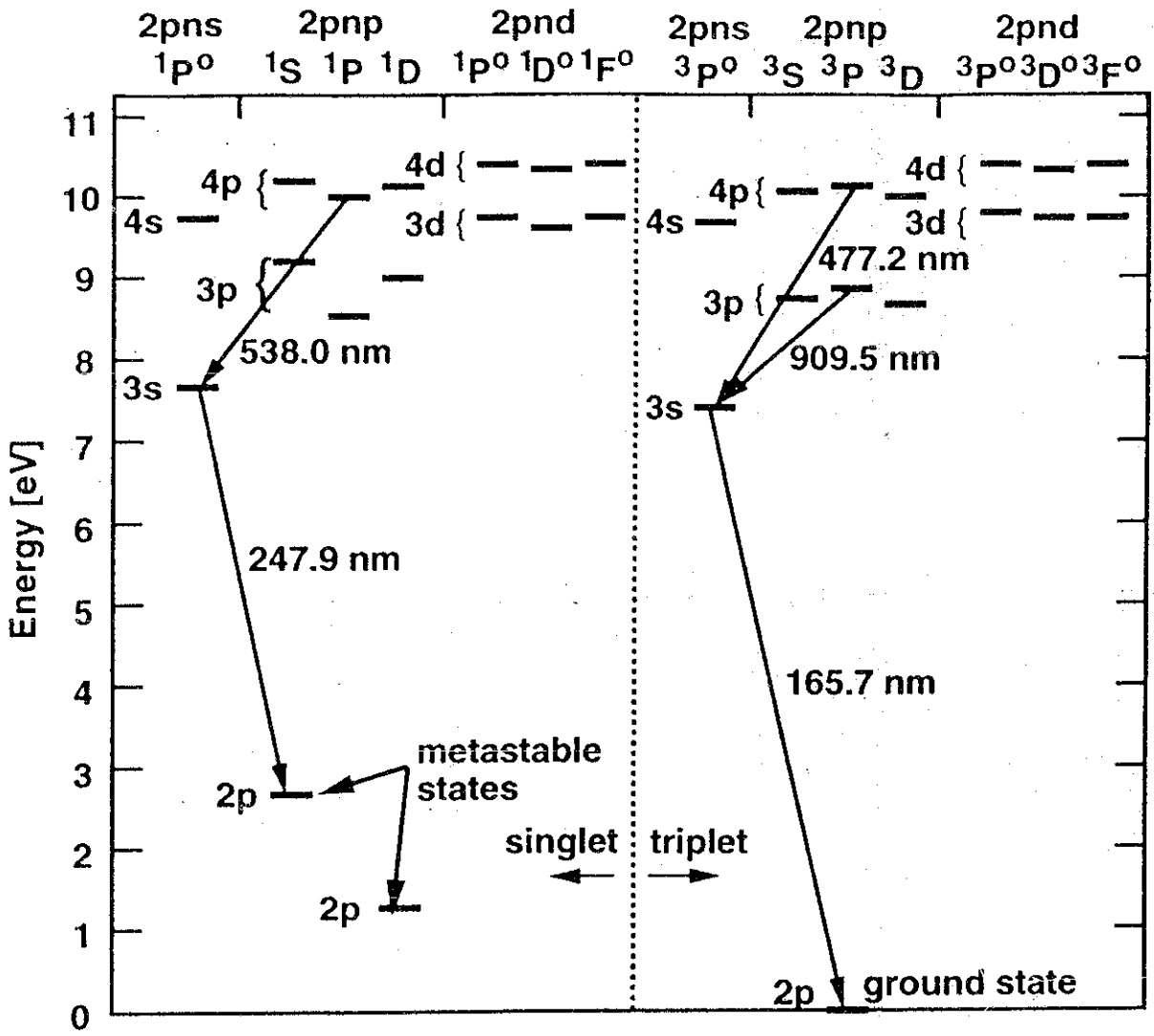
2pns
1Po
2pnp
1S 1P 1D
2pnd
1Po 1Do 1Fo
2pns
3Po
2pnp
3S 3P 3D
2pnd
3Po 3Do 3Fo
Energy [eV]
11
10
9
8
7
6
5
4
3
2
1
0
4p
4s
3p
3s
2p
4d
3d
538.0 nm
247.9 nm
metastable
states
2p
singlet
triplet
477.2 nm
909.5 nm
165.7 nm
2p
ground state

Fig. 1

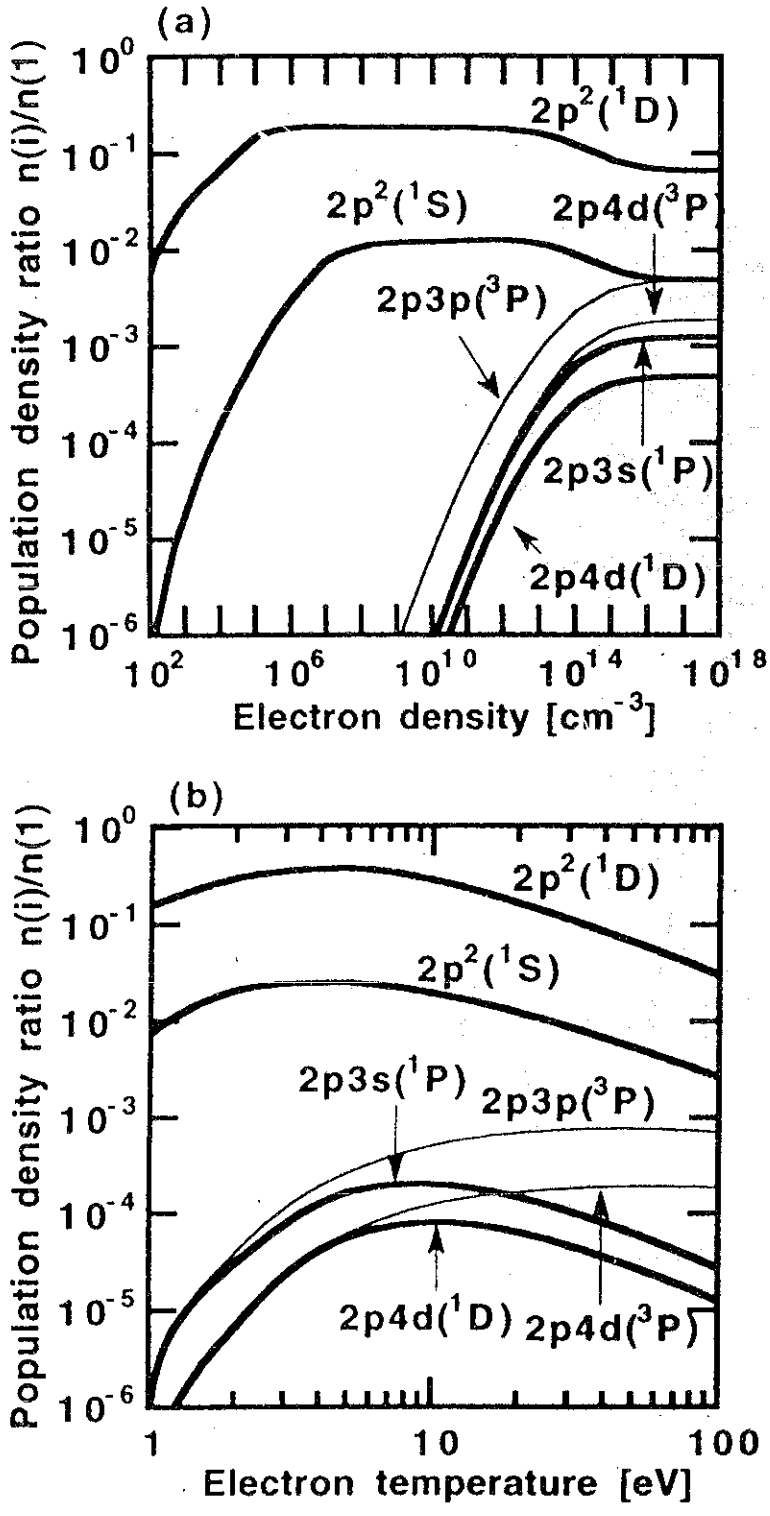
(a)
Population density ratio n(i)/n(1)
10^{0}
10^{-1}
10^{-2}
10^{-3}
10^{-4}
10^{-5}
10^{-6}
$2p^2(^1D)$
$2p^2(^1S)$
$2p4d(^3P)$
$2p3p(^3P)$
$2p3s(^1P)$
$2p4d(^1D)$
10^{2}
10^{6}
10^{10}
10^{14}
10^{18}
Electron density [cm^{-3}]
(b)
Population density ratio n(i)/n(1)
10^{0}
10^{-1}
10^{-2}
10^{-3}
10^{-4}
10^{-5}
10^{-6}
$2p^2(^1D)$
$2p^2(^1S)$
$2p3s(^1P)$
$2p3p(^3P)$
$2p4d(^1D)$
$2p4d(^3P)$
1
10
100
Electron temperature [eV]

Fig. 2

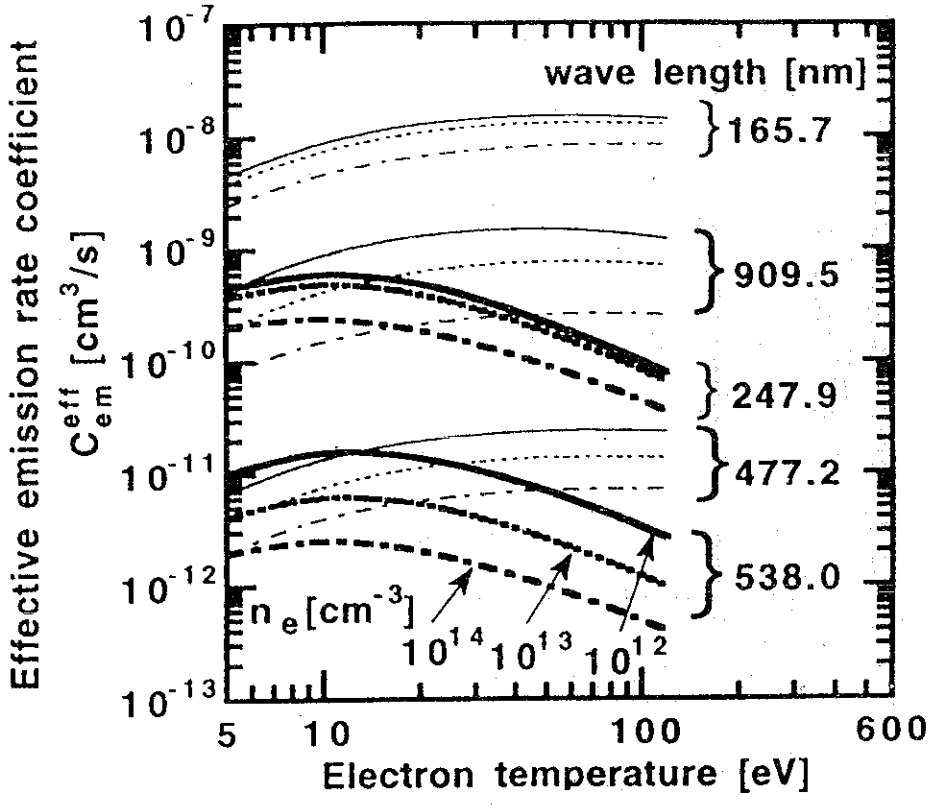
Effective emission rate coefficient
C_{em}^{eff} [cm^3/s]
wave length [nm]
165.7
909.5
247.9
477.2
538.0
n_e [cm^{-3}]
10^{14} 10^{13} 10^{12}
Electron temperature [eV]

Fig. 3

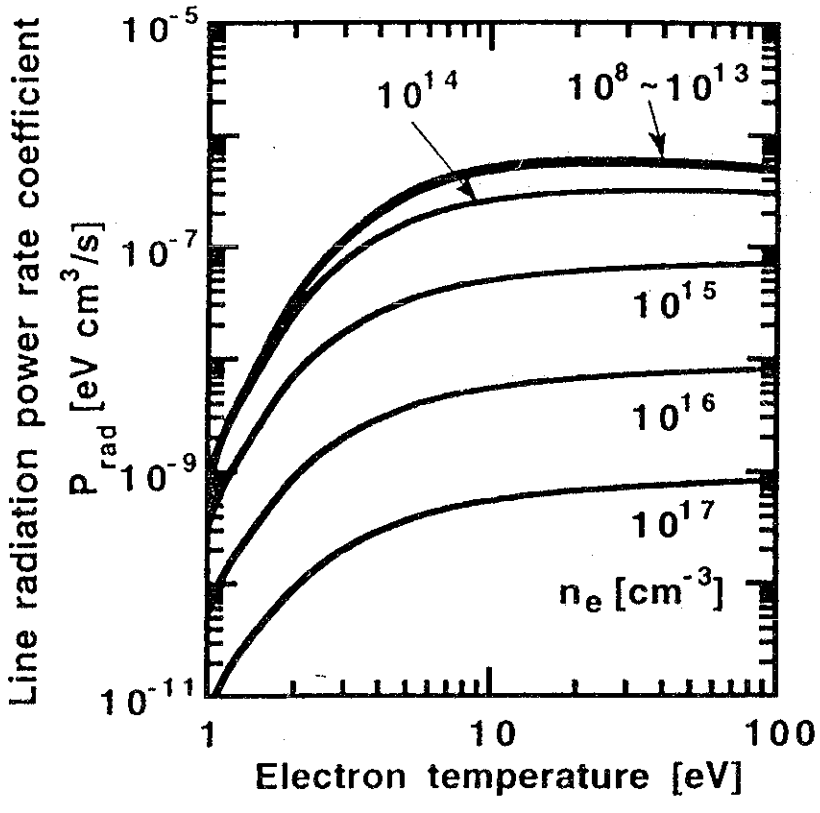
Line radiation power rate coefficient
P_{rad} [eV cm^3/s]
10^{14}
10^8 ~ 10^{13}
10^{15}
10^{16}
10^{17}
n_e [cm^{-3}]
Electron temperature [eV]

Fig. 4

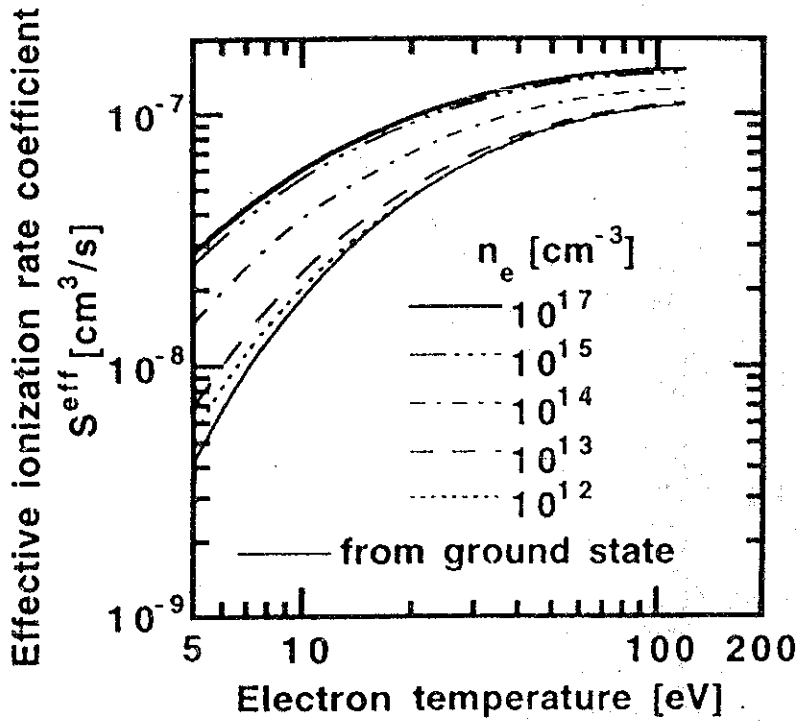
Effective ionization rate coefficient
S^{eff} [cm^3/s]
10^{-7}
10^{-8}
10^{-9}
n_e [cm^{-3}]
10^{17}
10^{15}
10^{14}
10^{13}
10^{12}
from ground state
5
10
100
200
Electron temperature [eV]

Fig. 5

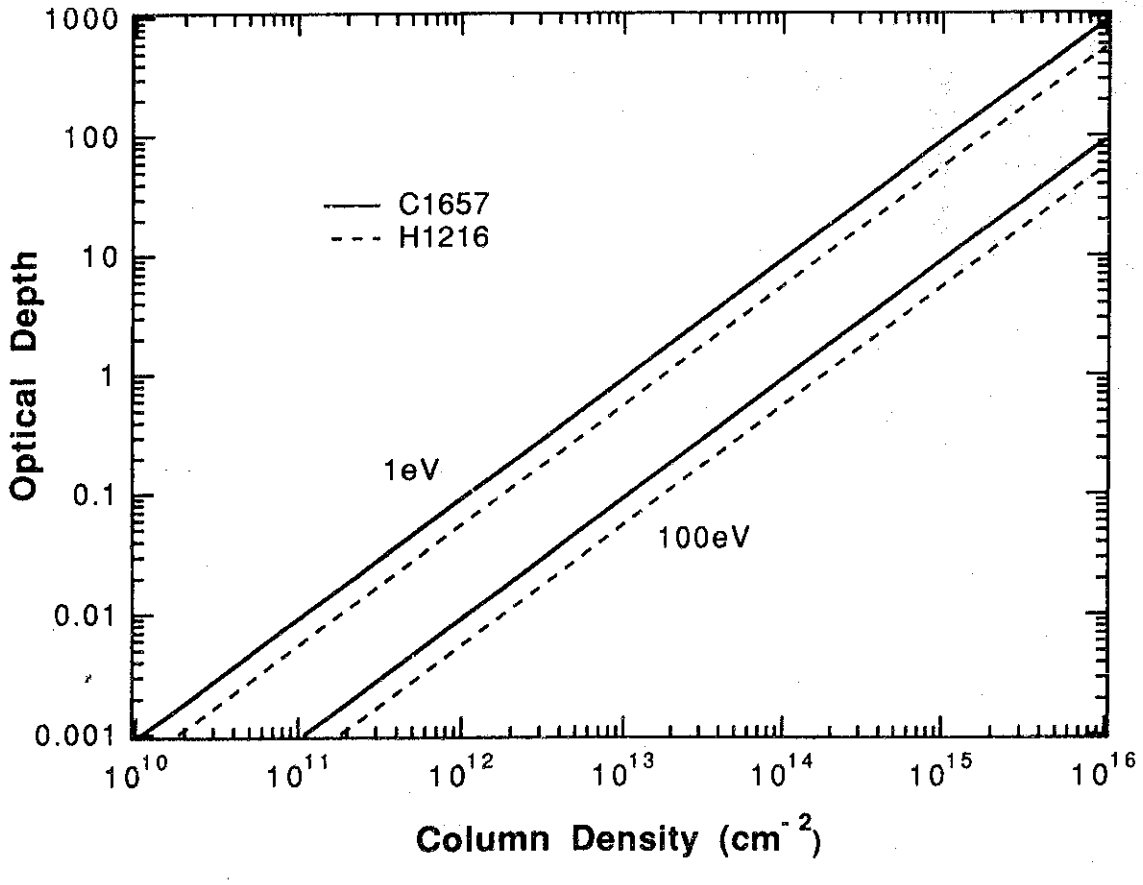
1000
100
10
1
0.1
0.01
0.001
Optical Depth
C1657
H1216
1eV
100eV
10^{10}
10^{11}
10^{12}
10^{13}
10^{14}
10^{15}
10^{16}
Column Density (cm^{-2})

Fig. 6

NIFS-MEMOシリーズ出版リスト
(Recent Issues of NIFS-MEMO Series)

NIFS-MEMO-1 都築哲哉、東井和夫、松浦清剛、「パソコンによる JIPP T-IIU プラズマの平衡位置フィードバック制御」1991年 4月
T.Tsuzuki, K.Toi and K.Matsuura, "Feedback Control of Plasma Equilibrium with Control System Aided by Personal Computer on the JIPP T-II Tokamak" ; Apr.1991 (In Japanese)

NIFS-MEMO-2 久保田雄輔、大林治夫、宮原 昭、大野和子、中村光一、堀井憲爾、「環境磁界の研究 (I) 三次元積分磁束計の開発」1991年 7月
Y.Kubota, H.Obayashi, A.Miyahara, K.Ohno, K.Nakamura and K.Horii, "Development of Three-Dimensional Compact Magnetic Dosimeter for Environmental Magnetic Field Monitoring" , July,1991 (In Japanese)

NIFS-MEMO-3 「核融合科学研究所技術研究会; 1991年3月19、20日 土岐文化プラザ」1991年8月
"Proceedings of Symposium on Technology in Laboratories; Mar. 19, 20, 1991" Aug. 1991 (In Japanese)

NIFS-MEMO-4 「プラズマ中におけるカオス現象」1991年8月
"Chaotic Phenomena in Plasmas " , Aug. 1991 (In Japanese)

NIFS-MEMO-5 山崎耕造、「ファジー論理のトロイダルプラズマ制御への応用」1992年2月
"Fuzzy Logic Application to Troidal Plasma Contol " , Feb. 1992 (In Japanese)

NIFS-MEMO-6 平成３年度 核融合科学研究所 支援調査共同研究報告書 「大出力マイクロ波源の開発に関する調査研究」1992年4月
"Development of High Power Microwave Source " , Apr. 1992 (In Japanese)

NIFS-MEMO- 7 平成３年度 核融合科学研究所 共同研究（調査支援研究）研究成果報告書 「プラズマにおけるカオス現象」1992年11月
"Chaotic Phenomena in Plasma, II" , Nov. 1992 (In Japanese)

NIFS-MEMO-8 NIFSシンポジウム報告書「核融合炉材料照射用強力中性子源の設計と大学の役割」1993年1月
"Design of Intense Neutron Source for Fusion Material Study and the Role of Universities" , Jan. 1993 (In Japanese)

NIFS-MEMO-9 平成２、３、４年度 核融合科学研究所共同研究研究会研究成果報告書 「開放磁場における電位と輸送機構」１９９３年４月
(Ed.) K. Yatsu and T. Hatori
"Potential Formation and Transport in Open Field Line Systems" , Apr. 1993 (In Japanese)

NIFS-MEMO-10 伊藤公孝、「人口太陽は燃えるか ー核融合研究最前線ー原子力オープン・スクール講演」１９９３年５月
K. Itoh
Reports of NIFS Collaboration Workshop from 1990 to 1992 at National Institute for Fusion SCience.
"At the Front of Fusion Research -Introductory Lecture Open to Public-" , May 1993 (In Japanese)